

Similarity-Dissimilarity Loss for Multi-label Supervised Contrastive Learning

Guangming Huang¹, Yunfei Long¹, Cunjin Luo¹, Sheng Liu²

¹School of Computer Science and Electronic Engineering, University of Essex, UK

²Department of Gastrointestinal Surgery, Xiangya Hospital, Central South University, China

¹{gh22231, yl20051, cunjin.luo}@essex.ac.uk

Abstract

Supervised contrastive learning has been explored in making use of label information for multi-label classification, but determining positive samples in multi-label scenario remains challenging. Previous studies have examined strategies for identifying positive samples, considering label overlap proportion between anchors and samples. However, they ignore various relations between given anchors and samples, as well as how to dynamically adjust the weights in contrastive loss functions based on different relations, leading to great ambiguity. In this paper, we introduce five distinct relations between multi-label samples and propose a Similarity-Dissimilarity Loss with contrastive learning for multi-label classification. Our loss function re-weights the loss by computing the similarity and dissimilarity between positive samples and a given anchor based on the introduced relations. We mainly conduct experiments for multi-label text classification on MIMIC datasets, then further extend the evaluation on MS-COCO. The Experimental results show that our proposed loss effectively improves the performance on all encoders under supervised contrastive learning paradigm, demonstrating its effectiveness and robustness.

1 Introduction

Multi-label classification is a challenging and arduous classification task due to its label correlation, extreme and sparse label space and long-tailed distribution. For instance, in the International Classification of Diseases (ICD) (Edin et al., 2023), the presence of one label (e.g., "Pneumococcal pneumonia") may increase the likelihood of other labels (e.g., "fever" or "cough"). Additionally, multi-label datasets often exhibit a long-tailed distribution, where some labels are very common while others are rare. This imbalance can result in models that perform well on frequent labels but poorly on infrequent ones (Zhang et al., 2023). The number

of potential label combinations increases exponentially with the number of labels, leading to high computational complexity and substantial memory usage.

Supervised contrastive learning effectively utilizes label information to achieve promising results in single-label classification (Khosla et al., 2020). Nevertheless, how to properly identify positive samples in multi-label scenario remains challenging compared to single-label classification. For example, given a set of images of cats and puppies and an anchor image of a cat, it is straightforward to identify positive and negative samples based on the provided label information. However, for multi-label classification, determining whether an image containing both a cat and a puppy should be considered a positive or negative sample introduces ambiguity.

An important question arises: *Should a sample be considered positive when its label set partially overlaps with or exactly matches the anchor's?* Currently, there are three mainstream strategies for identifying positive samples in multi-label scenario (Zhang and Wu, 2024): 1) **ALL** considers only samples with an exactly matching label set as positive, 2) **ANY** identifies samples with any overlapping class with the anchor as positive, and 3) **MulSupCon** (Zhang and Wu, 2024) defines positive samples similarly to ANY but considers each label separately, forming multiple positive sets for a single anchor sample.

However, these methods have inherent limitations, since previous studies have overlooked relations between samples and anchors for multi-label contrastive learning paradigm. As illustrated in Figure 1, we introduce five distinct set relations between samples and anchors. ALL considers only $R2$ and disregards contributions of $R3$, $R4$ and $R5$. Moreover, in long-tail distribution, when tail samples are used as anchors, ALL's reliance on exact label matches makes it difficult for these tail

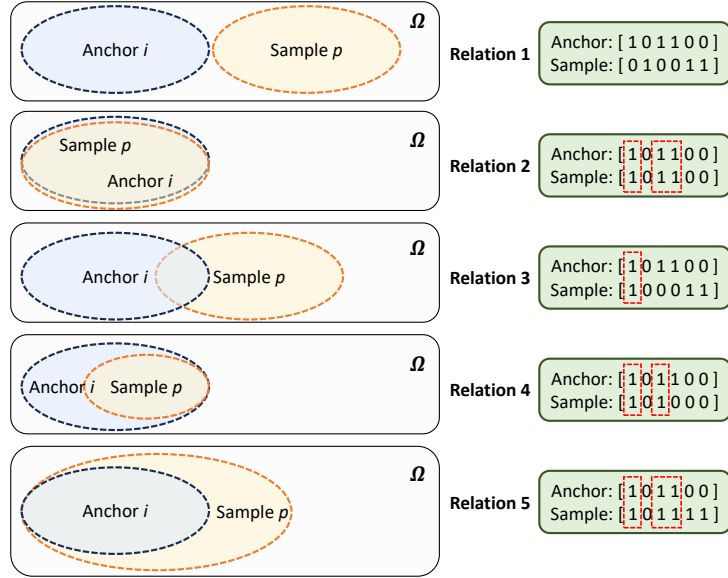


Figure 1: Five distinct relations between samples and a given anchor. Ω denotes a universe that contains all label entities. Here is an example with five different relations between sample p and anchor i , where the labels are represented as one-hot vectors.

anchors to find positive samples within a limited batch, potentially degenerating the method to unsupervised contrastive learning in extreme cases. For ANY and MulSupCon, $R2$, $R3$, $R4$ and $R5$ are treated identically with the same weights in the contrastive loss. These two approaches are clearly suboptimal since these four relations are different. We will further analyze these three methods mathematically in detail in section 2.

To the best of our knowledge, we are the first to introduce five distinct relations for multi-label contrastive learning paradigm. Based on these relations, we propose Similarity-Dissimilarity Loss with Supervised contrastive learning for multi-label classification, which re-weighting the loss by the similarity and dissimilarity between samples and anchors.

2 Methods

In this section, we study the limitations of ALL, ANY and MulSupCon based on the five distinct relations. Then we present the Similarity-Dissimilarity Loss and mathematically prove effectiveness of our loss function.

2.1 Preliminaries

Given a batch of N randomly sample/label pairs, $\{(\mathbf{x}_i, \mathbf{y}_i)\}_{i=1\dots N}$, where \mathbf{x}_i and \mathbf{y}_i represent the i -th sample and its labels individually. $\mathbf{y}_i = \{y_i^{(l)}\}_{l=1\dots L}$ is the multi-labels of sample i , where

$y_i^{(l)}$ denotes the l -th label of sample i and L is the size of labels of sample i . The corresponding batch used for training consists of $2N$ pairs after data augmentation, $\{\tilde{\mathbf{x}}_j, \tilde{\mathbf{y}}_j\}_{j=1\dots 2N}$, where $\tilde{\mathbf{x}}_{2i}$ and $\tilde{\mathbf{x}}_{2i-1}$ are two random augmentations of \mathbf{x}_i ($i = 1\dots N$) and $\tilde{\mathbf{y}}_{2i-1} = \tilde{\mathbf{y}}_{2i} = \mathbf{y}_i$. For a reminder, we will refer to a set of $2N$ augmented samples as a "batch" to be more brief (Khosla et al., 2020).

2.2 Multi-label Supervised Contrastive Loss

For multi-label classification, the formulation of supervised contrastive loss varies depending on the strategies used to determine positive samples for a given anchor. Let $i \in \mathcal{I} = \{1\dots 2N\}$ represent the index of an arbitrary augmented sample. The positive set for ALL is defined as follows:

$$\mathcal{P}(i) = \{p \in \mathcal{A}(i) | \forall p, \tilde{\mathbf{y}}_p = \tilde{\mathbf{y}}_i\} \quad (1)$$

and the positive set for ANY is defined as follows:

$$\mathcal{P}(i) = \{p \in \mathcal{A}(i) | \forall p, \tilde{\mathbf{y}}_p \cap \tilde{\mathbf{y}}_i \neq \emptyset\} \quad (2)$$

where $\mathcal{A}(i) \equiv \mathcal{I} \setminus \{i\}$.

Correspondingly, in multi-label supervised contrastive learning using the ALL and ANY strategies, the loss function for each anchor i is expressed as follows:

$$\mathcal{L}_i = \frac{-1}{|\mathcal{P}(i)|} \sum_{p \in \mathcal{P}(i)} \log \frac{\exp(\mathbf{z}_i \cdot \mathbf{z}_p / \tau)}{\sum_{a \in \mathcal{A}(i)} \exp(\mathbf{z}_i \cdot \mathbf{z}_a / \tau)} \quad (3)$$

Here, $\tau \in \mathbb{R}^+$ is a scalar temperature parameter (Chen et al., 2020), $\mathbf{z}_k = \text{Proj}(\text{Enc}(\tilde{\mathbf{x}}_k)) \in \mathbb{R}^{D_P}$ (Khosla et al., 2020).

For a batch, the loss function is written as:

$$\mathcal{L} = \sum_{i \in I} \mathcal{L}_i \quad (4)$$

Zhang and Wu (2024) consider each label $\tilde{y}_i^{(l)}$ separately, forming multiple positive sets for an anchor sample i . For each $\tilde{y}_i^{(l)} \in \tilde{\mathbf{y}}_i$, the positive set for **MulSupCon** is defined as:

$$\mathcal{P}(i) = \{p \in \mathcal{A}(i) \mid \forall p, \tilde{y}_p^{(l)} \in \tilde{\mathbf{y}}_i\} \quad (5)$$

For each anchor i , the multi-label supervised contrastive loss for MulSupCon is represented as follows (Zhang and Wu, 2024):

$$\mathcal{L}_i^{Mul} = \sum_{\tilde{y}_p^{(l)} \in \tilde{\mathbf{y}}_i} \frac{-1}{|\mathcal{P}(i)|} \sum_{p \in \mathcal{P}(i)} \log \frac{\exp(\mathbf{z}_i \cdot \mathbf{z}_p / \tau)}{\sum_{a \in \mathcal{A}(i)} \exp(\mathbf{z}_i \cdot \mathbf{z}_a / \tau)} \quad (6)$$

For one batch, the loss function is written as:

$$\mathcal{L}^{Mul} = \frac{1}{\sum_i |\tilde{\mathbf{y}}_i|} \sum_{i \in I} \mathcal{L}_i^{Mul} \quad (7)$$

2.3 Five Distinct Relations in Multi-label

As shown in Figure 1, we denote each *Relation* as R , where, e.g., $R1$ stands for *Relation 1*. The notation p_j indicates that the sample p belongs to the j -th relation.

Given a universe Ω that contains all label entities, let \mathcal{S} represent the set of labels for anchor i and let \mathcal{T} denote the set of labels for sample p . The five relations are defined as follows:

$$R1 : \mathcal{S} \cap \mathcal{T} = \emptyset \quad (8)$$

$$R2 : \mathcal{S} = \mathcal{T} \quad (9)$$

$$R3 : \mathcal{S} \cap \mathcal{T} \neq \emptyset, \mathcal{S} \not\subseteq \mathcal{T}, \mathcal{T} \not\subseteq \mathcal{S} \quad (10)$$

$$R4 : \mathcal{S} \supseteq \mathcal{T} \quad (11)$$

$$R5 : \mathcal{S} \subseteq \mathcal{T} \quad (12)$$

Based on the definitions of the relations, we theoretical analyze the limitations of ALL, ANY and MulSupCon with an example in Figure 1

For ALL, the optimization is directed toward the mean representation of all samples with exactly the same labels (Zhang and Wu, 2024). As the case illustrated in Figure 1, given anchor i , the positive set is:

$$\mathcal{P}(i) = \{p_2\}$$

In ALL, p_j in $R2$ is considered as positive sample, while the contributions of p_j in $R3$, $R4$ and $R5$ are disregarded. As a result, the size $|\mathcal{P}(i)|$ is limited, leading to a mean representation that suffers from randomness. Additionally, ALL treats samples belonging to the same class as negative in some cases.

Proposition 1. Given an anchor i , suppose that any sample p has labels $\tilde{y}_p = \tilde{y}_i$, according to the similarity calculation between a positive sample and a given anchor in contrastive learning (Chen et al., 2020), the projected vector \mathbf{z}_i is similar with vector \mathbf{z}_p , written as $\mathbf{z}_i \simeq \mathbf{z}_p$.

As per ANY's definition, the positive set is

$$\mathcal{P}(i) = \{p_2, p_3, p_4, p_5\}$$

By Proposition 1, the loss of p_j in Equation 3 is

$$\mathcal{L}(R2) \approx \mathcal{L}(R3) \approx \mathcal{L}(R4) \approx \mathcal{L}(R5)$$

It is evident that $R2$, $R3$, $R4$ and $R5$ represent distinct relations, each characterized by different labels and information. However, the ANY method fails to distinguish these fine-grained label differences, leading to significant ambiguity and lack of clarity. Furthermore, another drawback of this approach is that when most samples share common classes, the averaging process tends to emphasize the information of these common classes, thereby reducing the contribution of others (Zhang and Wu, 2024).

For MulSupCon, positive samples are identified similarly to ANY, with p_j in $R2$, $R3$, $R4$ and $R5$ being considered positive. However, MulSupCon distinguishes itself by evaluating each label individually and forming multiple positive sets for a single anchor sample. This approach aggregates positive samples based on the number of overlapping labels between the positive samples and the anchor, thereby expanding the space of positive sets:

$$\mathcal{P}(i) = \{p_2, p_2, p_2, p_3, p_4, p_4, p_5, p_5, p_5\}$$

Subsequently, the loss for p_j in Equation 6 are as follows by Proposition 1:

$$\mathcal{L}(R2) \approx \mathcal{L}(R5) \neq \mathcal{L}(R3) \neq \mathcal{L}(R4)$$

In this case, while MulSupCon successfully distinguishes $R3$ and $R4$ from $R2$ and $R5$, it fails

¹We are cautious in using the approximate sign instead of the equal sign since the absence of a rigorous mathematical proof in deep learning "blackbox".

to differentiate between *R2* and *R5*. The primary reason is that MulSupCon de facto considers the overlapping regions (i.e., intersecting portions) between sample p and anchor i , while neglecting the non-intersecting regions (see Figure 1).

2.4 Similarity-Dissimilarity Loss

To address the aforementioned issues, we introduce the concepts of similarity and dissimilarity in based on definitions the relations: (1) As shown in Figure 1, *Similarity* refers to the intersection regions (i.e., $\mathcal{S} \cap \mathcal{T}$), and (2) *Dissimilarity* refers to the non-intersecting regions with respect to sample p (i.e., $\mathcal{T} - \mathcal{S} \cap \mathcal{T}$). For each anchor i , Similarity-Dissimilarity Loss is written as follows:

$$\mathcal{L}_i^{our} = \frac{-1}{|\mathcal{P}(i)|} \sum_{p \in \mathcal{P}(i)} \log \frac{\mathcal{K}_{i,p}^s \mathcal{K}_{i,p}^d \exp(\mathbf{z}_i \cdot \mathbf{z}_p / \tau)}{\sum_{a \in \mathcal{A}(i)} \exp(\mathbf{z}_i \cdot \mathbf{z}_a / \tau)} \quad (13)$$

Here, $\mathcal{K}_{i,p}^s$ denotes the Similarity, and $\mathcal{K}_{i,p}^d$ indicates the Dissimilarity with respect to sample p . They are respectively defined as:

$$\mathcal{K}_{i,p}^s = \frac{|\tilde{\mathbf{y}}_p^s|}{|\tilde{\mathbf{y}}_i|} = \frac{|\mathcal{S} \cap \mathcal{T}|}{|\mathcal{S}|} \quad (14)$$

and

$$\mathcal{K}_{i,p}^d = \frac{1}{1 + |\tilde{\mathbf{y}}_p^d|} = \frac{1}{1 + |\mathcal{T} - \mathcal{S} \cap \mathcal{T}|} \quad (15)$$

where $|\tilde{\mathbf{y}}_i| = |\mathcal{S}|$ represents the size of label space of $\tilde{\mathbf{y}}_i$, $|\tilde{\mathbf{y}}_p^s| = |\mathcal{S} \cap \mathcal{T}|$ represents the size of the intersection, and $|\tilde{\mathbf{y}}_p^d| = |\mathcal{T} - \mathcal{S} \cap \mathcal{T}|$ denotes the size of non-intersecting regions with respect to sample p . It is worth noting that:

$$0 \leq |\tilde{\mathbf{y}}_p^d| = |\tilde{\mathbf{y}}_p| - |\tilde{\mathbf{y}}_p^s| \quad (16)$$

where $|\tilde{\mathbf{y}}_p|$ denotes the size of label space of sample p .

Specifically, the Similarity-Dissimilarity Loss is a generalized version of Equation 3, when $|\tilde{\mathbf{y}}_i| = |\tilde{\mathbf{y}}_p^s|$ and $|\tilde{\mathbf{y}}_p^d| = 0$.

2.4.1 Case Analysis

We analyze our loss function using the example of five different relations in Figure 1, $|\tilde{\mathbf{y}}_{p_j}^s| = \{0, 3, 1, 2, 3\}_{j=1,2,3,4,5}$, and $|\tilde{\mathbf{y}}_{p_j}^d| = \{3, 0, 2, 0, 2\}_{j=1,2,3,4,5}$, then $\mathcal{K}_{i,p}^s = \{0, 1, \frac{1}{3}, \frac{2}{3}, 1\}$

in Equation 14 and $\mathcal{K}_{i,p}^d = \{\frac{1}{4}, 1, \frac{1}{3}, 1, \frac{1}{3}\}$ in Equation 15, and then $\mathcal{K}_{i,p}^s \mathcal{K}_{i,p}^d = \{0, 1, \frac{1}{9}, \frac{2}{3}, \frac{1}{3}\}$. Correspondingly, the loss of p_j in Equation 13 correspond to:

$$\mathcal{L}(R2) \neq \mathcal{L}(R3) \neq \mathcal{L}(R4) \neq \mathcal{L}(R5)$$

In this case, our proposed loss function successfully differentiates the five distinct relations by re-weighting the loss as outlined in Equation 13, 14 and 15.

Moreover, compared to MulSupCon, Similarity-Dissimilarity Loss maintain the size of positive sets, resulting no necessities to require extra computation cost

2.4.2 Theoretical Analysis

Our proposed loss function aim to re-weight the loss by the combination of the factors $\mathcal{K}_{i,p}^s$ and $\mathcal{K}_{i,p}^d$, thus, $\mathcal{K}_{i,p}^s \mathcal{K}_{i,p}^d$ is supposed to be on the interval $[0, 1]$ based on various relations.

To be more brief, we use $\{\mathcal{K}_m^s \mathcal{K}_m^d\}_{m=1,2,3,4,5}$ to represent the combination of the Similarity and Dissimilarity factors in the five relations.

Proposition 2. If $m = 1$, then $\mathcal{K}_m^s \mathcal{K}_m^d = 0$.

Proof. If $m = 1$, then $\mathcal{S} \cap \mathcal{T} = \emptyset$, hence, $|\tilde{\mathbf{y}}_p^s| = |\mathcal{S} \cap \mathcal{T}| = 0$, we have:

$$\mathcal{K}_1^s \mathcal{K}_1^d = 0 \quad (17)$$

Proposition 3. If $m = 2$, then $\mathcal{K}_m^s \mathcal{K}_m^d = 1$.

Proof. If $m = 2$, then $\mathcal{S} = \mathcal{T}$, combining Equation 14 and 15, we have $\mathcal{K}_2^s = \frac{|\mathcal{S} \cap \mathcal{T}|}{|\mathcal{S}|} = 1$ and $\mathcal{K}_2^d = \frac{1}{1 + |\mathcal{T} - \mathcal{S} \cap \mathcal{T}|} = 1$. Therefore,

$$\mathcal{K}_2^s \mathcal{K}_2^d = 1 \quad (18)$$

Proposition 4. If $m = \{3, 4, 5\}$, then $1 > \mathcal{K}_m^s \mathcal{K}_m^d > 0$.

Proof. If $m = \{3, 4, 5\}$, then $\mathcal{S} \cap \mathcal{T} \neq \emptyset$ and $\mathcal{S} \neq \mathcal{T}$. Since $|\mathcal{S}| > 0$, then $\mathcal{K}_m^s \neq 0$ and $\mathcal{K}_m^d \neq 0$. Let $m = 3$, applying Equation 10, we have $|\mathcal{S} \cap \mathcal{T}| < |\mathcal{S}|$, and then $\mathcal{K}_3^s < 1$. Meanwhile, $|\mathcal{T} - \mathcal{S} \cap \mathcal{T}| > 0$, then $\mathcal{K}_3^d < 1$. Thus, $1 > \mathcal{K}_3^s \mathcal{K}_3^d > 0$.

Similarly, $\mathcal{K}_4^s < 1$ and $\mathcal{K}_4^d = 1$, $\mathcal{K}_5^s = 1$ and $\mathcal{K}_5^d < 1$. Thus, $1 > \mathcal{K}_4^s \mathcal{K}_4^d > 0$ and $1 > \mathcal{K}_5^s \mathcal{K}_5^d > 0$

Summarizing:

$$\mathcal{K}_2^s \mathcal{K}_2^d = 1 > \mathcal{K}_m^s \mathcal{K}_m^d > 0 = \mathcal{K}_1^s \mathcal{K}_1^d, m = 3, 4, 5 \quad (19)$$

	MIMIC-III-Full	MIMIC-III-50
Train	47,723	8,066
Val	1,631	1,573
Test	3,372	1,729
Avg # codes [†]	15.7	5.7
Total # codes	8,692	50
	IV-ICD9-Full	IV-ICD9-50
Train	188,533	170,664
Val	7,110	6,406
Test	13,709	12,405
Avg # codes [†]	13.4	4.7
Total # codes	11,145	50
	IV-ICD10-Full	IV-ICD10-50
Train	110,442	104,077
Val	4,017	3,805
Test	7,851	7,368
Avg # codes [†]	16.1	5.4
Total # codes	25,230	50

Table 1: Statistics of MIMIC-III and MIMIC-IV datasets under full/top-50 and ICD-9/ICD-10 codes settings. [†] indicates the average of ICD codes for each record in the training set.

3 Experiments

3.1 Datasets and Metrics

We mainly conduct the experiments for multi-label text classification on MIMIC datasets, which feature an extremely large label space and exhibit a long-tail distribution (Huang et al., 2024). Our experiments are performed under both full (long-tail distribution) and top-50 settings (non-long-tail distribution), allowing us to effectively assess the impact of our loss function across different data distributions. Long-tail distribution is particularly prevalent in multi-label tasks. Moreover, we extend the experiments on MS-COCO for further evaluation

MIMIC. The MIMIC-III ² dataset (Johnson et al., 2016) includes records labeled with expert-annotated ICD-9 codes, which identify diagnoses and procedures. The MIMIC-IV ³ dataset (Johnson et al., 2020) contains records annotated with both ICD-9 and ICD-10 codes, where each code is subdivided into sub-codes that often capture specific circumstantial details. We adhere to the same splits as in previous works (Mullenbach et al.,

²We are granted access to MIMIC-III Clinical Database (v1.4)

³We are granted access to MIMIC-IV (v2.2)

2018), employing two settings: MIMIC-III-Full, which includes all ICD-9 codes, and MIMIC-III-50, which includes only the 50 most frequent codes. For the MIMIC-IV dataset, we follow prior studies (Nguyen et al., 2023) and utilize four settings: MIMIC-IV-ICD9-Full, MIMIC-IV-ICD9-50, MIMIC-IV-ICD10-Full, and MIMIC-IV-ICD10-50. The statistics for the MIMIC-III and MIMIC-IV datasets with these six settings are presented in Table 1.

MS-COCO dataset (Lin et al., 2014) comprises 80 object categories, ranging from common household items to animals and vehicles. It consists of 164K images, divided into training (83K), validation (41K), and test (41K) sets.

Metrics. Consistent with prior research (Mullenbach et al., 2018; Nguyen et al., 2023), we report Macro/Micro-AUC, Macro/Micro-F1, and precision at K ($P@K$) metrics, where $K = \{1, 5, 8\}$ for different settings.

3.2 Baselines and Encoders

We compare our proposed loss function against three baseline functions: 1) ALL, 2) ANY, and 3) MuSupCon (Zhang and Wu, 2024), within the multi-label supervised contrastive learning framework.

The evaluation utilizes a diverse set of encoders:

- For non-pretrained language models (non-PLMs), we employ a CNN architecture following Mullenbach et al. (2018).
- For pretrained language models (PLMs), we use the base configurations of BERT (Devlin et al., 2019), RoBERTa (Liu et al., 2019), ELECTRA (Clark et al., 2019) and XLNet (Yang et al., 2019) to ensure parameter consistency with PLM-ICD. Notably, XLNet is an autoregressive model, distinguishing it from the other selected PLMs.
- To further assess the effectiveness of our loss function on PLMs with domain-specific knowledge, we incorporate BioBERT (Lee et al., 2020) and PLM-ICD (Huang et al., 2022) as encoders.
- For image data, we follow Zhang and Wu (2024) and use ResNet-50 as the encoder.

3.3 Implementation Details

Within the supervised contrastive learning framework, we adhere to a two-step training process as

	MIMIC-III-Full						MIMIC-IV-ICD10-Full					
	AUC		F1		Precision		AUC		F1		Precision	
	Macro	Micro	Macro	Micro	P@8	Macro	Micro	Macro	Micro	P@8	Macro	Micro
CNN+ALL	80.4	94.5	4.8	42.0	57.9	86.1	96.2	3.2	47.2	59.6		
+ANY	78.2	90.2	3.1	40.9	54.0	84.0	95.0	3.1	45.4	58.1		
+MulSupCon	81.8	95.0	5.9	43.1	59.0	87.0	97.1	3.5	48.0	60.5		
+Our	83.0	95.8	6.8	44.0	60.2	87.7	97.6	3.7	48.8	61.4		
BERT+ALL	89.5	95.4	7.8	53.0	70.6	89.7	98.6	4.1	52.7	64.3		
+ANY	88.1	93.8	7.1	51.1	68.8	88.9	98.0	3.9	51.4	63.3		
+MulSupCon	90.2	96.0	8.5	53.7	71.0	90.0	98.6	4.2	53.6	65.0		
+Our	90.5	96.5	8.8	54.2	71.3	90.2	98.7	4.4	54.3	65.7		
RoBERTa+ALL	89.8	95.8	7.9	53.0	71.0	89.4	98.1	4.2	53.8	64.1		
+ANY	88.1	94.1	7.1	51.3	68.9	89.0	98.0	4.0	52.2	62.6		
+MulSupCon	90.3	96.3	8.6	54.1	71.2	90.5	98.7	4.5	54.0	65.4		
+Our	90.7	96.6	9.1	54.6	71.3	90.6	98.8	4.7	54.8	66.0		
ELECTRA+ALL	90.0	96.1	8.4	53.8	71.4	89.2	98.3	3.9	53.9	64.4		
+ANY	88.7	94.6	8.1	52.2	69.3	89.2	97.8	3.7	51.9	62.9		
+MulSupCon	90.9	97.0	9.1	54.8	71.7	90.4	98.5	4.6	53.9	65.7		
+Our	91.4	97.2	9.2	55.0	72.5	90.7	98.7	4.8	54.7	66.3		
XLNet+ALL	89.8	96.0	7.9	52.7	71.3	89.7	98.3	4.4	54.0	64.4		
+ANY	88.3	94.2	7.2	51.0	68.6	88.9	97.8	4.1	52.1	62.9		
+MulSupCon	90.1	96.5	8.8	54.2	71.2	90.3	98.4	4.5	54.3	65.4		
+Our	90.4	96.8	8.8	54.8	71.2	90.7	98.5	4.7	55.2	66.1		
BioBERT+ALL	90.5	96.3	8.9	54.1	71.9	89.4	98.8	4.3	54.1	64.9		
+ANY	88.9	95.1	8.5	52.4	69.6	89.6	98.1	4.0	52.4	63.1		
+MulSupCon	91.3	97.5	9.3	55.1	72.0	90.9	98.9	4.6	54.2	66.0		
+Our	91.9	97.6	9.5	55.3	72.9	91.2	99.0	4.9	54.9	66.8		
PLM-ICD +ALL	92.5	98.6	10.7	60.0	76.8	91.8	98.7	4.8	57.3	69.2		
+ANY	91.0	97.3	9.2	58.8	75.3	90.5	97.7	4.5	55.8	68.1		
+MulSupCon	93.4	99.1	11.6	61.4	77.6	92.8	99.3	5.4	58.1	70.1		
+Our	94.4	99.4	12.4	62.3	78.4	93.7	99.5	5.7	58.7	70.7		

Table 2: Results on the MIMIC-III-Full and MIMIC-IV-ICD10-Full test sets. The best scores among encoders modeling are marked in **bold**.

outlined by [Khosla et al. \(2020\)](#): 1) First, we train an encoder to generate vector representations of inputs, ensuring that representations of texts or images belonging to the same class are more similar to each other than those from different classes; 2) Subsequently, we train a classifier using the frozen encoder. Our implementation builds on the Huggingface platform ([Wolf et al., 2020](#)) and utilizes end-to-end training.

For MIMI-III and MIMIC-IV datasets, we employ the AdamW optimizer ([Loshchilov and Hutter, 2018](#)) in combination with a linear learning rate scheduler with a warmup ratio of $1e - 4$. A batch size of 128 is applied for MIMIC datasets with all settings. Given that the average record length in the MIMIC datasets is approximately 1,000 tokens,

we search the input max length for the encoders of $\{512, 1024\}$ tokens. For MS-COCO datasets, we follow [Zhang and Wu \(2024\)](#)’s hyperparameter settings, training the model through the SGD optimizer with an initial learning rate of 0.1 and a cosine learning rate scheduler. A batch size of 64 is utilized for MS-COCO. We apply a random crop to the images, resizing them to 224×224 pixels, followed by color jittering and random conversion to greyscale. Additionally, an early stopping mechanism is implemented, terminating the training process if the F1 score on the validation set shows no improvement over 6 consecutive epochs. Importantly, we ensured consistency in hyperparameters when comparing models using the same encoder.

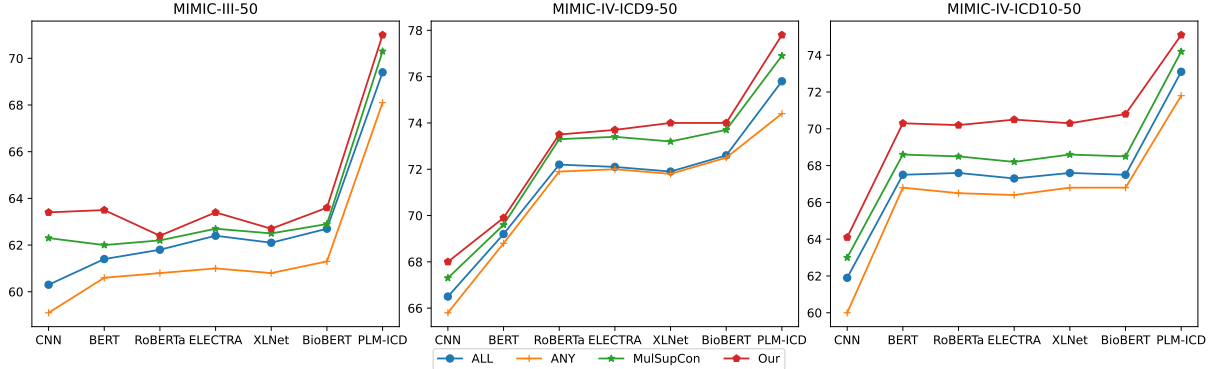


Figure 2: Results on MIMIC-III-50, MIMIC-IV-ICD9-50 and MIMIC-IV-ICD10-50 test sets. Micro-F1 score (%) is used as the metric.

	CNN	BERT	RoBERTa	ELECTRA	XLNet	BioBERT	PLM-ICD
MIMIC-III-Full							
C-to-ALL	2.0	1.2	1.6	1.2	2.1	1.2	2.3
C-to-ANY	3.1	3.1	3.3	2.8	3.8	2.9	3.5
C-to-Mul	0.9	0.5	0.5	0.2	0.6	0.2	0.9
MIMIC-IV-ICD9-Full							
C-to-ALL	1.8	0.7	1.1	0.6	0.6	1.0	2.1
C-to-ANY	2.5	1.0	1.4	1.2	1.3	1.6	3.1
C-to-Mul	0.8	0.4	0.2	0.2	0.3	0.5	0.7

Table 3: Comparisons of Micro-F1 score (%) between our proposed loss and baselines on ICD-9 full setting. The comparisons of our loss with ALL, ANY and MulSupCon denote C-to-ALL, C-to-ANY and C-to-Mul, respectively.

4 Results and Analysis

Overall, as demonstrated by the experimental results (see Table 2, 3 and 4, and Figure 2), our proposed contrastive loss function consistently outperforms ALL, ANY, and MulSupCon across all evaluation metrics. The application of our loss function enhances the performance of all encoders within the supervised contrastive learning paradigm. The results indicate that our loss function is effective across diverse datasets, including both text and image data, as well as various data distributions, such as long-tailed and non-long-tailed distributions.

Main Results. As shown in Table 2, we compare our proposed loss function with ALL, ANY, and MulSupCon on the MIMIC-III (ICD-9) and MIMIC-IV (ICD-10) datasets under the full setting, characterized by an extremely large label space and long-tail distribution. The results demonstrate that our loss function consistently outperforms ALL, ANY, and MulSupCon across all evaluation metrics and encoders, including non-PLM (e.g., CNN), PLMs (BERT, RoBERTa, ELECTRA and XLNet), and domain-specific PLMs (BioBERT and

PLM-ICD). Notably, our loss function achieves the same 8.8% of Macro-F1 as MulSupCon on XLNet compared to MulSupCon. MIMIC-IV-ICD10-Full, with its significantly larger set of 25,230 codes compared to MIMIC-III-Full’s 8,692 codes (see Table 1), presents a particularly challenging scenario due to the complexity and additional information contained in ICD-10 codes compared to ICD-9 (WHO, 1948). Despite these challenges, our loss function continues to demonstrate effectiveness and robustness on the MIMIC-IV-ICD10-Full dataset.

Non-long-tailed Distribution Settings. We analyze the Micro-F1 scores of all loss functions using the top 50 settings across MIMIC-III and MIMIC-IV datasets. As illustrated in Figure 2, our proposed function consistently demonstrates superior performance of Micro-F1 compared to the baselines on all datasets. The results indicate that encoders play a critical role in contrastive learning, with PLMs like BERT outperforming non-PLMs such as CNN. Furthermore, incorporating domain-specific pre-training knowledge significantly enhances model performance.

	Macro-F1	Micro-F1	Precision@1
ALL	60.2	65.8	89.3
ANY	54.0	62.1	87.9
MulSupCon	63.2	68.3	91.2
Our	65.3	70.2	92.8

Table 4: Experimental results on MS-COCO dataset. We compare our loss function with ALL, ANY and MulSupCon on ResNet-50.

Analysis on ICD-9. To further validate the effectiveness of our proposed loss function, we analyze its performance on MIMIC-III and MIMIC-IV under the same ICD-9 full setting. As demonstrated in Table 3, our loss function steadily exceeds the baseline methods in terms of Micro-F1 score. However, the performance improvement on MIMIC-IV is relatively modest compared to MIMIC-III. This discrepancy may be attributed to the larger label space of MIMIC-IV and the fact that its training dataset is approximately 4 times the size of MIMIC-III, thereby reducing the impact of the loss function within the contrastive learning paradigm.

Effectiveness on Image Data. To demonstrate that our proposed loss function is not only effective for text data but also generalizes well to image data. As shown in Table 4, our function surpasses ALL, ANY and MulSupCon, especially, with a significant improvement of 2.1/1.9/1.6 in Macro-F1/Micro-F1/Precision@1, respectively. It is worth noting that our experimental results are slightly lower than those reported by (Zhang and Wu, 2024), likely due to the end-to-end training method employed, while Zhang and Wu (2024) applied a momentum training method (He et al., 2020).

5 Related Work

Contrastive learning aims to learn a representation of data such that similar instances are close together in the representation space, while dissimilar instances are far apart. Compared to self-supervised contrastive methods, such as SimCLR (Chen et al., 2020) and MoCo (He et al., 2020), Khosla et al. (2020) introduced supervised contrastive learning, which makes full use of label information to further enhance the performance under contrastive learning paradigm. Recent studies have extended supervised contrastive learning from single-label to multi-label settings by leveraging label information. Zhang et al. (2022) introduced a hierarchical multi-label representation learning framework designed

to utilize all available labels while maintaining the hierarchical relationships among classes. Additionally, they proposed hierarchy-preserving losses that impose a hierarchical penalty on the contrastive loss, thereby enforcing hierarchical constraints. In a subsequent study, Zhang and Wu (2024) developed Multi-Label Supervised Contrastive Learning (MulSupCon), which features a contrastive loss function that expanding the space of positive sets based on the overlap proportion

However, the intricate relationships and dependencies between multi-label samples have yet to be fully elucidated. To address this gap, we identify and introduce five distinct relations between samples and anchors. Inspired by the idea of re-weighting of logit adjustment (Menon et al., 2021), focal loss (Lin et al., 2017) and class-balanced loss (Cui et al., 2019), we leverage the combination of similarity and dissimilarity factor to re-weight the contrastive loss.

6 Conclusion

Multi-label classification poses a compelling challenge in applying contrastive learning due to the diverse ways of defining relations between multi-label samples. In this paper, we introduce five distinct relations between samples and the given anchors. Leveraging these relations, we propose a Similarity-Dissimilarity Loss with supervised contrastive learning for multi-label classification, which dynamically re-weights the loss by the combination of similarity and dissimilarity factor. We compare our loss function with three baselines (ALL, ANY and MulSupCon). Robust results evaluated with five metrics suggest the effectiveness of our proposed contrastive loss.

The introduction of these relations elucidates the complex correlations between samples and anchors in multi-label contrastive learning, offering a more refined approach for determining positive samples and exploring label correlations. Furthermore, our proposed loss function addresses the challenge of enabling models to better learn multi-label representations by dynamically adjusting penalties in intricate multi-label scenarios.

Limitations

This study introduces an effective loss function for multi-label classification by re-weighting the loss, but it is important to recognize its limitations. Currently, our proposed loss function is only applicable

to supervised contrastive learning and cannot be used in other learning paradigms, such as semi-supervised or unsupervised learning. Additionally, supervised contrastive learning is constrained by batch size during training and the data augmentation methods, which introduces certain limitations. Therefore, generalizing the proposed loss function to other learning paradigms or explore a general loss function for multi-label scenarios would be valuable avenues for future research. Moreover, compared to traditional single-label classification, multi-label classification presents additional challenges due to two key factors: label co-occurrence and the long-tailed distribution of labels. This study does not specifically address these two issues. Notably, the long-tailed distribution in multi-label scenarios is more complex due to label dependencies, and techniques such as re-sampling or re-balancing can introduce inter-class imbalances.

References

Ting Chen, Simon Kornblith, Mohammad Norouzi, and Geoffrey Hinton. 2020. A simple framework for contrastive learning of visual representations. In *International conference on machine learning*, pages 1597–1607. PMLR.

Kevin Clark, Minh-Thang Luong, Quoc V Le, and Christopher D Manning. 2019. Electra: Pre-training text encoders as discriminators rather than generators. In *International Conference on Learning Representations*.

Yin Cui, Menglin Jia, Tsung-Yi Lin, Yang Song, and Serge Belongie. 2019. Class-balanced loss based on effective number of samples. In *Proceedings of the IEEE/CVF conference on computer vision and pattern recognition*, pages 9268–9277.

Jacob Devlin, Ming-Wei Chang, Kenton Lee, and Kristina Toutanova. 2019. Bert: Pre-training of deep bidirectional transformers for language understanding. In *Proceedings of the 2019 Conference of the North American Chapter of the Association for Computational Linguistics: Human Language Technologies, Volume 1 (Long and Short Papers)*, pages 4171–4186.

Joakim Edin, Alexander Junge, Jakob D Havtorn, Lasse Borgholt, Maria Maistro, Tuukka Ruotsalo, and Lars Maaløe. 2023. Automated medical coding on mimic-iii and mimic-iv: a critical review and replicability study. In *Proceedings of the 46th International ACM SIGIR Conference on Research and Development in Information Retrieval*, pages 2572–2582.

Kaiming He, Haoqi Fan, Yuxin Wu, Saining Xie, and Ross Girshick. 2020. Momentum contrast for unsupervised visual representation learning. In *Proceedings of the IEEE/CVF conference on computer vision and pattern recognition*, pages 9729–9738.

Chao-Wei Huang, Shang-Chi Tsai, and Yun-Nung Chen. 2022. Plm-icd: Automatic icd coding with pretrained language models. In *Proceedings of the 4th Clinical Natural Language Processing Workshop*, pages 10–20.

Guangming Huang, Yingya Li, Shoaib Jameel, Yunfei Long, and Giorgos Papanastasiou. 2024. From explainable to interpretable deep learning for natural language processing in healthcare: How far from reality? *Computational and Structural Biotechnology Journal*, 24:362–373.

Alistair Johnson, Lucas Bulgarelli, Tom Pollard, Steven Horng, Leo Anthony Celi, and Roger Mark. 2020. Mimic-iv. *PhysioNet*. Available online at: <https://physionet.org/content/mimiciv/1.0/> (accessed August 23, 2021), pages 49–55.

Alistair EW Johnson, Tom J Pollard, Lu Shen, Li-wei H Lehman, Mengling Feng, Mohammad Ghassemi, Benjamin Moody, Peter Szolovits, Leo Anthony Celi, and Roger G Mark. 2016. Mimic-iii, a freely accessible critical care database. *Scientific data*, 3(1):1–9.

Prannay Khosla, Piotr Teterwak, Chen Wang, Aaron Sarna, Yonglong Tian, Phillip Isola, Aaron Maschinot, Ce Liu, and Dilip Krishnan. 2020. Supervised contrastive learning. *Advances in neural information processing systems*, 33:18661–18673.

Jinhyuk Lee, Wonjin Yoon, Sungdong Kim, Donghyeon Kim, Sunkyu Kim, Chan Ho So, and Jaewoo Kang. 2020. Biobert: a pre-trained biomedical language representation model for biomedical text mining. *Bioinformatics*, 36(4):1234–1240.

Tsung-Yi Lin, Priya Goyal, Ross Girshick, Kaiming He, and Piotr Dollár. 2017. Focal loss for dense object detection. In *Proceedings of the IEEE international conference on computer vision*, pages 2980–2988.

Tsung-Yi Lin, Michael Maire, Serge Belongie, James Hays, Pietro Perona, Deva Ramanan, Piotr Dollár, and C Lawrence Zitnick. 2014. Microsoft coco: Common objects in context. In *Computer Vision–ECCV 2014: 13th European Conference, Zurich, Switzerland, September 6–12, 2014, Proceedings, Part V 13*, pages 740–755. Springer.

Yinhan Liu, Myle Ott, Naman Goyal, Jingfei Du, Mandar Joshi, Danqi Chen, Omer Levy, Mike Lewis, Luke Zettlemoyer, and Veselin Stoyanov. 2019. Roberta: A robustly optimized bert pretraining approach. *arXiv preprint arXiv:1907.11692*.

Ilya Loshchilov and Frank Hutter. 2018. Decoupled weight decay regularization. In *International Conference on Learning Representations*.

Aditya Krishna Menon, Sadeep Jayasumana, Ankit Singh Rawat, Himanshu Jain, Andreas Veit, and Sanjiv Kumar. 2021. Long-tail learning via

logit adjustment. In *International Conference on Learning Representations*.

James Mullenbach, Sarah Wiegreffe, Jon Duke, Jimeng Sun, and Jacob Eisenstein. 2018. Explainable prediction of medical codes from clinical text. In *Proceedings of the 2018 Conference of the North American Chapter of the Association for Computational Linguistics: Human Language Technologies, Volume 1 (Long Papers)*, pages 1101–1111.

Thanh-Tung Nguyen, Viktor Schlegel, Abhinav Kashyap, Stefan Winkler, Shao-Syuan Huang, Jie-Jyun Liu, and Chih-Jen Lin. 2023. Mimic-iv-icd: A new benchmark for extreme multilabel classification. *arXiv preprint arXiv:2304.13998*.

WHO. 1948. International statistical classification of diseases and related health problems.

Thomas Wolf, Lysandre Debut, Victor Sanh, Julien Chaumond, Clement Delangue, Anthony Moi, Pierrette Cistac, Tim Rault, Rémi Louf, Morgan Funtowicz, et al. 2020. Transformers: State-of-the-art natural language processing. In *Proceedings of the 2020 conference on empirical methods in natural language processing: system demonstrations*, pages 38–45.

Zhilin Yang, Zihang Dai, Yiming Yang, Jaime Carbonell, Russ R Salakhutdinov, and Quoc V Le. 2019. Xlnet: Generalized autoregressive pretraining for language understanding. *Advances in neural information processing systems*, 32.

Pingyue Zhang and Mengyue Wu. 2024. Multi-label supervised contrastive learning. In *Proceedings of the AAAI Conference on Artificial Intelligence*, volume 38, pages 16786–16793.

Shu Zhang, Ran Xu, Caiming Xiong, and Chetan Ramaiah. 2022. Use all the labels: A hierarchical multi-label contrastive learning framework. In *Proceedings of the IEEE/CVF Conference on Computer Vision and Pattern Recognition*, pages 16660–16669.

Yifan Zhang, Bingyi Kang, Bryan Hooi, Shuicheng Yan, and Jiashi Feng. 2023. Deep long-tailed learning: A survey. *IEEE Transactions on Pattern Analysis and Machine Intelligence*, 45(9):10795–10816.